Lifetime of liquid metal wires for stretchable devices

Kristen L. Dorsey Nathan Lazarus*

Dr. Kristen L. Dorsey
Picker Engineering Program, Smith College, Northampton, MA, USA
Kristen@KristenDorsey.com
Dr. Nathan Lazarus
US Army Research Laboratory, Adelphi, MD, USA

Keywords: *Liquid metal, Galinstan, stretchable, soft robotics*

As stretchable devices become well established for applications in soft robotics and wearable devices, the compliant conductors that make these applications possible must also be reliable and survive for the entire device lifetime. Liquid metals such as Galinstan are a potential solution as non-toxic, stretchable, and low resistance conductors. Rigorous investigations of liquid metal lifetimes, however, are limited. This work presents the median lifetime of liquid metal-filled silicone tubes under current density on the order of 1 kAcm^{-2}, which is necessary for applications such as electromagnetic actuators. In these conductors, the median lifetime increases by a factor of over 4700 as current decreases from 2 kAcm^{-2} to 1 kAcm^{-2}. By cooling the sample, median failure time increased from 112 s to 9.4 h, which suggests straightforward solutions to maximize liquid metal wire lifetime by increasing thermal conductivity or by duty cycling the applied current.

Soft robotics seeks to reduce or eliminate the reliance on rigid material components, with the goal of realizing enhanced performance in tasks such as grasping [1] and manipulation [2], morphology and rigidity changes [3, 4], and safety over rigid manipulators [5, 6]. With notable exceptions [7, 8], these actuators depend on rigid components for control, which presents concerns for compliance mismatch between soft and rigid components. A promising material towards achieving "all-soft" platforms is Galinstan and other gallium alloys that are liquid at room temperature. When encapsulated by another soft material (e.g., silicone elastomer), these liquid metals retain high electrical conductivity while remaining mechanically compliant, soft, and stretchable. As liquid metals become established approaches for interconnect in soft-material platforms, characterizing the expected lifetimes under standard operating conditions will be essential to realizing "all-soft" robots and other devices.

Galinstan is a frequently chosen liquid metal for soft robotics applications due to its commercial availability, low toxicity and vapor pressure [9], high electrical conductivity [10], a self-terminating oxide layer [11], and selective wetting properties [9, 12]. In comparison to some stretchable conductive materials (e.g., particle-elastomer matrices [13]), Galinstan has low resistance and maintains its low resistance ($<$ 10 Ω) with deformation [14]. It can also be patterned using a range of approaches [15, 16], including stencil patterning [17, 18] two-dimensional [19] and three-dimensional printing [20] by extrusion, laser sintering [21], injection into patterned channels [22, 23], and selective wetting [24, 25].

Galinstan and other liquid metals have been widely demonstrated in applications such as sensing [22, 26, 27, 28], interconnect [20, 24], and antennas [29, 30], where the ability to withstand high current is not a consideration. However, liquid metals for select applications must tolerate higher currents to serve their intended functions. Joule heaters with liquid metals [3, 4, 31, 32, 33] have applications in inducing a phase change in variable stiffness actuators, where a material (e.g., Field's metal, polylactic acid) is heated above its solid phase transition temperature to change stiffness in the material. Current density J demonstrated in heating is on the order of 1 kAcm^{-2} (e.g., 0.80 kAcm^{-2} [31], 0.950 kAcm^{-2} [32]). Wireless power transfer with Galinstan has been used for device charging (J = 0.3 kAcm^{-2} [34], J = 1-20 kAcm^{-2} [35]) and wireless wearable devices [36]. Finally, silicone-encapsulated Galinstan serves as the stretchable coil for electromagnetic actuators in soft robots [37, 38], pumps [39], and loudspeakers [40], with demonstrated current densities from 0.05 kAcm^{-2} [37] to 10 kAcm^{-2} [38].

One application of electromagnetic actuators in soft robotics is as soft valves that can control fluidic elastomeric actuators [41, 42, 43]. A fluid (e.g., air) is pumped into the actuator, typically with pumps made of metals and rigid plastics. To realize an "all-soft" platform, these rigid-material components must be replaced with soft counterparts. Ideally, the soft-material replacements would survive for the anticipated lifetime of the actuator under the conditions required for operation.

The effects of high current density on liquid metals have been previously studied [44, 45, 46, 47], finding deleterious effects due to electromigration or thermal mechanisms. Electromigration has been well-

studied as a failure mechanism in solid metal [48, 49, 50]. Upon applying current, a metal ion in the conductive trace experiences a force towards the cathode proportional to its valence and a force towards the anode caused by momentum transfer from electrons to the ion. The mass transfer causes material migration outside of the trace, eventually resulting in an open circuit failure.
Median time to failure (MTTF) due to electromigration has been modeled empirically [49] by

$$MTTF = ACJ^{-2}exp(E_a/kT) \tag{1}$$

where A is the cross-sectional area, C is a material constant, E_a is the activation energy of ion diffusion, k is Boltzmann's constant, and T is the temperature. Parameters A, C, and E_a are typically fit to the MTTF.
Electromigration has been observed in micro- or nanoscale interconnects with current densities higher than 1 MAcm^{-2} [51]. In liquid metals, however, the effects of electromigration have been observed at lower current densities and at shorter timescales than in solid metals. Von Kleist-Retzow et al. demonstrated formation and manipulation of >20 μm diameter Galinstan spheres inside a scanning electron microscope with a current density of 50 kAcm^{-2} in less than 10 minutes [52]. Michaud and Lacour [45] applied current densities from $5 - 100$ Acm^{-2} to a liquid gallium-solid gold interconnect and measured MTTFs from 10^2 s to 10^{-2} s, which they attributed to electromigration and the formation of Ga-Au compounds. Similarly, Park et al. found that a current density on the order of 2 MAcm^{-2} prompted the breakdown of free-standing, additively manufactured gallium-indium alloy (i.e., EGaIn) structures [46]. The authors observed morphological and chemical changes in the structures. A corresponding increase in breakdown current density to 3 MAcm^{-2} was observed for EGaIn-carbon nanotube matrices [47].
The failure of such liquid metals could also be thermally induced. He et. al. [44] observed a "boiling"-like response within 200 s when exposing liquid metal to a current density on the order of 1 kAcm^{-2}. The bubble formation is attributed to air pockets trapped between the Galinstan's native oxide skin and the encapsulating surface, which expanded when heated and pinched off the Galinstan channel. Je and Lee [53] noticed void formation in Galinstan-silicone heaters created by larger expansion of the encapsulating silicone than the Galinstan. These voids caused an increase in channel resistance and eventually reached open circuit failure at temperatures above 80 °C.
An unaddressed characterization in these works is the lifetime of liquid metals with applied current densities over 1 kAcm^{-2} in stretchable media. Here, we demonstrate a soft-membrane electromagnetic actuator, characterize the lifetimes of Galinstan-filled silicone, identify potential failure mechanisms, and propose design guidelines for stretchable devices operating at high current densities.
To understand the current density required to control stretchable valves, we modeled and characterized a soft electromagnetic actuator with a stationary actuation coil and a flexible silicone membrane with an embedded cylindrical permanent magnet. A DC current was applied to the actuation coil (Fig. 1a), creating an attractive force between the permanent magnet and the actuation coil and displacement of the magnet towards the coil (Fig. 1b). The force on the magnet under actuation was simulated and measured for a current density of 0.8 kAcm^{-2} (Fig. 1c), indicating that the force minimum occurs when the coil distance is 0 mm (i.e., the center of the coil and center of the magnet are aligned). The displacement from unactuated to actuated states is approximately 2 mm. The applied actuation current of 0.8 kAcm^{-2} provides an impetus for studying device lifetime for current densities in th range of 1 kAcm^{-2}. Details on the coil fabrication and force modeling are given in Materials and Methods.
In stretchable platforms, instability in liquid metals could mean changes in wire resistance or stiffness. While we focus primarily on the electrical characteristics, the thermal behavior also has implications for Galinstan stability. The oxide skin of Galinstan is stable up to 500 °C [46], but commonly used silicone elastomers (e.g., Sylgard 184 [54], Ecoflex [55]) are not stable above $200 - 220$ °C, with reports of silicones vaporizing near 520 °C [56].
The simulated and measured thermal response of Galinstan samples is presented in Fig. 2. Constant DC current densities from $1 - 2$ kAcm^{-2} were applied to Galinstan-filled silicone tubes. The silicone temperature at 2 mm from the Galinstan (Fig. 2a) was measured with a thermocouple and simulated to predict the temperature of the silicone next to the Galinstan. Simulation details are available in the Materials

and Methods section.

The measured steady-state temperature (Fig. 2b) monotonically increases with applied current density. This response is expected from the relationship between applied power, current density, and steady-state temperature, $T \propto J^2R$, where R is the resistance of the Galinstan. An exponential fit for the 2 kAcm^{-2} sample is included because every sample failed before reaching its steady-state temperature. The temperature simulation at high convection (h=30 $Wm^{-2}K^{-1}$) agrees well with measured temperatures. Fig. 2c shows the temperature over time as current density is stepped at time $t = 0$ from 0 A to its final value. The thermal time constants are approximately 120 s, such that each sample reaches its steady-state temperature around 600 s.

The simulation serves as a tool to ensure that the encapsulating silicone is not heated above its thermal decomposition temperature. At high convective heat transfer (h = 30 $Wm^{-2}K^{-1}$), the modeled temperature reaches 200 °C at an input current density of 1.8 kAcm^{-2}, while at low convective heat transfer (h = 10 $Wm^{-2}K^{-1}$), the silicone reaches this temperature at 1.55 kAcm^{-2}. While test conditions and device geometry will affect the steady-state temperature and time constants, this simulation suggests that 1.5 kAcm^{-2} is the maximum safe current density for 0.5 mm^2 cross-section wires.

The electrical characteristics and MTTF of Galinstan wires were characterized by applying constant DC current (Fig. 3a) until a voltage greater than 2.5 V was reached across the sample, indicating electrical failure. Fig. 3b are photographs of the wires before test and after open-circuit failure. Fig. 3c is a series of infrared thermographs showing wire temperature from the onset of current application until failure at 108 s. Further details describing experimental conditions and sample fabrication are included in the Materials and Methods section.

After failure, several samples have visible $1 - 3$ mm long gaps in the center of the liquid metal. Some samples (e.g., 1.75 kAcm^{-2} A) have twisted or buckled out of the encapsulating silicone. The bottom-most wire in the 1 kAcm^{-2} sample also shows texturing that initially became visible days before failure occurred and was present three days after completion of the test. These voids are less visible six days after test conclusion. The physical changes and gap formation before failure agree with infrared thermographs of the sample (Fig. 3b). Just before failure, the sample has a hotspot that appears over 45 s before failure and corresponds to the location of the gap after failure.

Fig. 4a are representative plots of the voltage across each wire as time progressed. Each sample shows an increase in voltage before failure, with the voltage increasing abruptly by more than 50 mV before failure in many samples. The lifetime of each sample and the MTTFs are presented in Fig. 4b, with the standard deviations σ of 540100 s (150 h), 197100 s (55 h), 38100 s (10.6 h), 57300 s (16 h), and 35 s for the 1 kAcm^{-2} through 2 kAcm^{-2} tests, respectively. The wire lifetimes are compared using Kaplan-Meier curves (Fig. 4c) over five minutes, two days, and two weeks. The Kaplan-Meier curve, which is used to demonstrate a population's survival probability after an event [57], is a method for comparing lifetimes when data do not fall into a modal distribution.

Across the applied current density range, MTTF decreases monotonically with current, with a factor increase of over 4700 from shortest median (112 s, 2 kAcm^{-2}) to longest median (148 h, 1 kAcm^{-2}). While all 2 kAcm^{-2} samples fail before 300 s, many samples with applied current density of 1.75 kAcm^{-2} A and 1.5 kAcm^{-2} show both early failures that occur within minutes to an hour and later failures that occur from several hours to several days. The 1 kAcm^{-2} samples all show lifetimes above 100 h, with two samples remaining conductive past the experimental cutoff time of 2 weeks (336 h).

Additional samples were tested using a ramp from 1 kAcm^{-2} to 2 kAcm^{-2} over 20 min and a periodic step between 0 Acm^{-2} and 2 kAcm^{-2} at a period of 20 s (root-mean-square current density of 1.4 kAcm^{-2}). Samples were also placed on a heat sink (i.e., passive cooling) and the cool side of a Peltier element (i.e., active cooling) under a continuous current of 2 kAcm^{-2}.

In contrast to the samples with 2 kAcm^{-2} applied (MTTF of 112 s), the ramped samples had lower MTTF (13 s, σ = 23 s), while the passively-cooled samples showed slightly higher MTTF (138 s, σ = 17700 s). One passively-cooled sampled remained conductive for over 12 h before the test was stopped due to an over-temperature fault. The actively-cooled samples showed higher MTTF (39900 s, σ = 30400 s), with one sample surviving beyond 150 h. The periodically pulsed test MTTF was 14.1 h (50600 s, σ=33300

s), or a factor of 450 increase over the 2 kAcm^{-2} samples.

By identifying the responsible failure mechanism(s), device lifetime could be extended through design or current application. We hypothesize that multiple mechanisms cause failure, and that these mechanisms fall into two categories: electromigration and thermal expansion. The sharp decline in MTTF with increasing current density suggests an electrical or thermal failure mechanism.

Several mechanisms could be at work in thermal failure. The volumetric coefficient of thermal expansion (CTE) for Galinstan is 1.15 $\times 10^{-4}$ K^{-1} [58], while polydimethyl siloxane (PDMS) expands volumetrically at 3.4 $\times 10^{-4}$ K^{-1} [59]. When heated, if the silicone expanded more than the Galinstan, voids would be created because Galinstan does not wet to the elastomer [18]. The remaining encapsulated Galinstan would bead up in the wire while other areas would be left with thinner Galinstan cross-sections. The thinner cross sections would have higher resistance and higher current density, increasing temperature locally and causing further expansion until a gap forms. With a CTE mismatch of 2.25 $\times 10^{-4}$ K^{-1} between Galinstan and silicone and a temperature increase of 120 K, the gap length between silicone and Galinstan would be approximately 0.5 mm, which is smaller than the gaps present at failure.

Another potential thermal failure mechanism is the presence of gas in the wire. Similarly to the behavior observed by He et al. [44], the gas may expand when heated and pinch off the Galinstan. Potential gas sources could be room air trapped between the silicone tubing and the oxide skin during fabrication, or vaporized silicone due to thermal decomposition, particularly at current densities above 1.5 kAcm^{-2}.

Modeling the MTTF with electromigration offers additional insight into the failure mechanisms. Normalizing the MTTF to the lowest value eliminates the fitting parameters A and C that are present in electromigration models, requiring only the value of activation energy and sample temperature. The measured MTTF at each current density, normalized to the MTTF at $J = 2$ kAcm^{-2} (Fig. 5a), shows a factor of 10^4 increase from the largest to the smallest current density. Modeling the expected increase in normalized MTTF with Eqn. 1 and an activation energy of 0.5 eV (that of small-crystalline solid Al [49]) results in a normalized MTTF factor of 10^3 across the current density range. A lower activation energy, as anticipated for liquid metals, reduces the normalized MTTF factor further. For electromigration to be a cause of failure across the current density range, the Galinstan activation energy would need to be much higher than that of solid, small-crystalline Al. Fig. 5b is plots of the predicted change in MTTF as temperature is decreased. For the $J = 2$ kAcm^{-2} samples, reducing sample temperature by 35 °C should only increase MTTF by a factor of two. However, actively cooling the sample increased MTTF by a factor of more than 450. Electromigration does not fully explain the observed behavior.

The formation of gaps in the wire centers, evidence of thermal expansion and wire deformation, the presence of hot spots that are visible in infrared imaging, and the divergent MTTF with cooling at 2 kAcm^{-2} support thermal failure as the mechanism. Cooling the samples does result in a large lifetime increase. Of particular note is that in the pulsed current trials, where effective current density is 1.4 kAcm^{-2}, the MTTF falls between the 1.25 kAcm^{-2} and 1.5 kAcm^{-2} continuous current median lifetimes. This behavior suggests that temperature, rather than the effects of current directly, plays the primary role in failure.

Additionally, if thermal mechanism(s) were responsible, the failure would likely occur before the steady-state temperature is reached (i.e., before 600 s). Indeed, 75% and 100% of failures occur before 600 s in the 1.75 and 2 kAcm^{-2} current densities, respectively.

Whether thermal failures are caused by void formation or pinchoff remains less clear. The thermal expansion mismatch between silicone and Galinstan is large enough to satisfactorily explain the presence of gaps in the wire at current densities above 1.5 kAcm^{-2}, but the gaps are larger than expected and there are inconsistencies in failure time. Some 1.5 kAcm^{-2} and 1.75 kAcm^{-2} samples survived well beyond the thermal settling time but failed hours or days later, as did all 1 and 1.25 1.5 kAcm^{-2} samples. The voids are also present long after the samples return to room temperature. Fabrication variations in silicone thickness may explain why some devices survive while others experience early failure. Variation in the fabrication process that introduce different air volumes might also explain the discrepancies between longer and shorter lifetimes.

Reducing the temperature of the wire is critical. Incorporating heat sinks or active cooling into actua-

tors requires changes to the system design. For applications such as stretchable electromagnetic valve actuation, where a continuous current may not be required, the most straightforward approach is simply by duty cycling the current. This approach satisfies the ability to operate at high current while extending wire lifetime. For heating and applications that require continuous current, careful attention to increasing thermal conduction (e.g., by reducing encapsulation thickness) may extend lifetime without sacrificing performance.
The lifetimes of Galinstan wires with 1-2 $kAcm^{-2}$ of applied current density suggest that multiple mechanisms influence stability and lifetime. For current densities between 1 and 1.25 $kAcm^{-2}$, electromigration-related mechanisms appear to be the primary cause of failure, while at 2 $kAcm^{-2}$, thermally-induced rupture or pinch-off causes failure. In the 1.5 and 1.75 $kAcm^{-2}$ samples, both thermal mechanisms, which cause early failure, and electromigration, which causes later failures, appear to be at work.
Characterizing and predicting the stability and lifetime of materials used within soft robotics and other soft-material platforms is a critical step in bringing these devices from the lab and into daily life. We estimated the lifetime of Galinstan wires under the same material and current conditions that are likely to occur under use. The potential for wires to survive beyond two weeks at current densities of 1 $kAcm^{-2}$ offers promise for their future use in robust, stable, and stretchable devices.

Materials and Methods

Experimental conditions

Galinstan samples were placed on a bed of dry, medium-coarse sand at room temperature (22 °C) and room humidity. Power was supplied to the samples from a benchtop power supply (9201, B&K Precision) controlled by LabView software. To measure wire voltage until open circuit failure, DC current was stepped from 0 A to a constant current at $t = 0$ while the voltage was measured at a sampling frequency of 10 Hz for the first 10,000 s and of 0.2 Hz afterwards. LabView was programmed to set the power supply to 0 A if an over-voltage condition (>2.5 V) was measured. Change in voltage was calculated by taking the voltage at t = 1 s as the initial voltage and subtracting it from measured voltage.
In the DC tests, the power supply was set to a constant current of 5, 6.25, 7.5 A, 8.75 A, or 10 A, which corresponded to $1 - 2$ $kAcm^{-2}$ in 0.25 $kAcm^{-2}$ increments. N samples were recorded for each current density (1 $kAcm^{-2}$, $N = 5$; 1.25 $kAcm^{-2}$, $N = 7$; 1.5 $kAcm^{-2}$, $N = 12$; 1.75 $kAcm^{-2}$, $N = 12$; 2 $kAcm^{-2}$, $N = 12$). The electrical failure time was defined as the point when the voltage increased above 2.5 V.
In the passively cooled heat sink tests ($N = 6$), the silicone sample was placed on an aluminum heatsink and current was sourced as described for DC conditions. In the active cooling tests ($N = 3$), the silicone sample was placed on a Peltier element (Laird CP2-127-10) with input power of 5.6 W, such that the initial temperature was 16 °C. In the ramp tests ($N = 3$), current remained at 5 A for 15 min before being stepped at a rate of 0.5 A every 30 seconds until 10 A was reached. In the pulse tests ($N = 4$), a square wave with 10 s of current on (10 A) and 10 s off (0 A) was sourced to each wire.
The thermal infrared images were taken with a Fluke IR camera (TiR) positioned at a height of 30 cm above the wire samples. The temperature of select samples was measured with a K-type thermocouple (5TC, Omega Engineering) embedded into the Ecoflex block parallel to the silicone tubes. The temperature was recorded with an Omega data-logger at a sampling frequency of 1 Hz.

Preparation of the stretchable electromagnet

A simple electromagnetic actuator was fabricated using a neodymium magnet (K and J Magnetics) with strength N52 (up to 14,800 G) using a previously described process [36]. Briefly, a mold with raised pillars is first manufactured in acrylonitrile butadiene styrene (ABS) using a Makerbot Replicator 2X. Fine gauge silicone tubing (HelixMark, inner diameter 0.31 mm, outer diameter 0.64 mm) is wrapped around the raised pillars to form the coil, followed by pouring Ecoflex 00-30 silicone to create the membrane and hold the silicone tubing in place. The tubing is filled with Galinstan using a syringe. Alternative fabrication approaches would also be possible, such as 3D printing the Galinstan coil directly [60]. The com-

pleted coil has ten turns and a diameter of roughly 15 mm. To connect to external wiring, copper wires were pushed into the ends of the silicone tubing without any additional sealing.

Preparation of the Galinstan samples

Galinstan was selected over other liquid metals due to its commercial availability and low toxicity. To fabricate the Galinstan wires, platinum-cure silicone tubes (0.035 in/0.8 mm inner diameter, McMaster-Carr) with a length of 7 cm were placed in pre-molded Ecoflex block (00-30, Reynolds Advanced Materials) and sealed with additional liquid Ecoflex, which is cured before Galinstan injection. Hypodermic needles (28 gauge, BD) were placed into the sealed ends of the tube and Galinstan (68.5% Ga, 21.5% In, 10% Sn, RotoMetals) was injected into the tube using a syringe. The sealed tubes prevent any Galinstan from leaking out of the tube during this step. 22 AWG copper wires with uninsulated length of 1 cm were placed into the tube ends after removal of the hypodermic needles, creating an effective silicone tube length of 5 cm. To seal and encapsulate the tubes and insertion point of the wires, a 1 mm thick Ecoflex cap was bonded to the topside of the Ecoflex tray.

Electromagnet modeling

The simulation of optimal distance between magnet and coil is derived from a previously demonstrated model [61]. Two conductive filaments, each carrying a current, experience a well-defined electromagnetic force between them. Both the electromagnetic actuation coil and an equivalent coil, modeling the permanent magnet, are treated as a series of individual filaments each carrying a known current. For the actuation coil, this current is applied through the coil; for the permanent magnet, it is a calculated current corresponding to the equivalent surface current density [61]. The total force then corresponds to a summation of the forces from all the filament combination pairs corresponding to the individual turns of the two coils.
The current density was calculated by dividing the applied current by the cross sectional area of the inner portion of the tubing, which corresponds to the Galinstan cross sectional area of the fabricated coil. Using a current density of 0.8 kAcm^{-2} as the current through the actuation coil, the forces on the permanent magnet were derived, resulting in a peak force greater than 60 mN at a separation of 2.5 mm between magnet and coil.

Temperature simulation

Input currents and dissipated powers were simulated using a three-dimensional finite element analysis (Comsol 5.3). The simulation used a 10 cm long, 0.8 mm diameter Galinstan trace (density ρ of 6440 kgm^{-3}, specific heat capacity c of 296 $Jkg^{-1}K^{-1}$ and thermal conductivity κ of 16.5 $Wm^{-1}K^{-1}$) encapsulated by silicone elastomer ($\rho = 1030\ kgm^{-3}$, $c = 1100\ Jkg^{-1}K^{-1}$, $\kappa = 0.27\ Wm^{-1}K^{-1}$) with thickness of 1.5 mm and placed on sand (ρ of 630 kgm^{-3}, $c = 800\ Jkg^{-1}K^{-1}$, $\kappa = 0.3\ Wm^{-1}K^{-1}$) with thickness of 50.8 mm to model the effects of an embedded wire resting on a bed of sand. Convective heat transfer was modeled above the elastomer block and below the sand with a heat transfer coefficient h of 10 $Wm^{-2}K^{-1}$ to 30 $Wm^{-2}K^{-1}$ to simulate the potential lower and upper ranges of convection.

Acknowledgements

This material is based upon work supported by the National Science Foundation under Grant No. 1846954. K.L. Dorsey would like to thank Eric Jensen and Dale Renfrow for assistance with silicone mold manufacturing and Miles Ott for guidance with Kaplan-Meier curves.

Conflict of Interest

The authors declare no conflicts of interest.

References

[1] R. Rocha, P. Lopes, A. d. Almeida, M. Tavakoli, C. Majidi, *Journal of Micromechanics and Microengineering* **2017**.

[2] W. Chen, H. Khamis, I. Birznieks, N. F. Lepora, S. J. Redmond, *IEEE Sensors Journal* **2018**, *18*, 22 9049, conference Name: IEEE Sensors Journal.

[3] Y. Hao, T. Wang, Z. Xie, W. Sun, Z. Liu, X. Fang, m. yang, L. Wen, *Journal of Micromechanics and Microengineering* **2017**.

[4] S. Rich, S.-H. Jang, Y.-L. Park, C. Majidi, *Advanced Materials Technologies* **2017**, *2*, 12 1700179.

[5] S. I. Rich, R. J. Wood, C. Majidi, *Nature Electronics* **2018**, *1*, 2 102.

[6] H. Abidi, M. Cianchetti, *Frontiers in Robotics and AI* **2017**, *4*, publisher: Frontiers.

[7] C. D. Onal, X. Chen, G. M. Whitesides, D. Rus, In H. I. Christensen, O. Khatib, editors, *Robotics Research : The 15th International Symposium ISRR*, Springer Tracts in Advanced Robotics, 525–540. Springer International Publishing, **2017**.

[8] M. Wehner, R. L. Truby, D. J. Fitzgerald, B. Mosadegh, G. M. Whitesides, J. A. Lewis, R. J. Wood, *Nature* **2016**, *536*, 7617 451.

[9] X. Zhao, S. Xu, J. Liu, *Frontiers in Energy* **2017**, 1–33.

[10] M. D. Dickey, *Advanced Materials* **2017**, *29*, 27 1606425.

[11] M. D. Dickey, In J. A. Rogers, R. Ghaffari, D.-H. Kim, editors, *Stretchable Bioelectronics for Medical Devices and Systems*, 3–30. Springer International Publishing, **2016**.

[12] R. K. Kramer, C. Majidi, R. J. Wood, *Advanced Functional Materials* **2013-11-13**, *23*, 42 5292.

[13] S. Wu, J. Zhang, R. B. Ladani, A. R. Ravindran, A. P. Mouritz, A. J. Kinloch, C. H. Wang, *ACS Applied Materials & Interfaces* **2017**, *9*, 16 14207, publisher: American Chemical Society.

[14] J.-B. Chossat, Y.-L. Park, R. J. Wood, V. Duchaine, *IEEE Sensors Journal* **2013**, *13*, 9 3405, conference Name: IEEE Sensors Journal.

[15] I. D. Joshipura, H. R. Ayers, C. Majidi, M. D. Dickey, *Journal of Materials Chemistry C* **2015**, *3*, 16 3834, publisher: The Royal Society of Chemistry.

[16] M. a. H. Khondoker, D. Sameoto, *Smart Materials and Structures* **2016**, *25*, 9 093001, publisher: IOP Publishing.

[17] N. Lazarus, S. S. Bedair, I. M. Kierzewski, *ACS Applied Materials & Interfaces* **2017-01-06**.

[18] J. Liu, S. Yang, Z. Liu, H. Guo, Z. Liu, Z. Xu, C. Liu, L. Wang, *Journal of Micromechanics and Microengineering* **2019-06**, *29*, 9 095001.

[19] M. G. Mohammed, R. Kramer, *Advanced Materials* **2017-02-01**, n/a–n/a.

[20] C. Votzke, U. Daalkhaijav, Y. Mengüç, M. L. Johnston, *IEEE Sensors Journal* **2019**, *19*, 10 3832 .

[21] S. Liu, M. C. Yuen, E. L. White, J. W. Boley, B. Deng, G. J. Cheng, R. Kramer-Bottiglio, *ACS Applied Materials & Interfaces* **2018-08-22**, *10*, 33 28232, publisher: American Chemical Society.

[22] K. L. Dorsey, M. Cao, G. A. Slipher, N. Lazarus, *IEEE Sensors Journal* **2018-09**, *18*, 18 7505.

[23] Y. Huang, Y. Wang, L. Xiao, H. Liu, W. Dong, Z. Yin, *Lab on a Chip* **2014-09-30**, *14*, 21 4205.

[24] K. B. Ozutemiz, J. Wissman, O. B. Ozdoganlar, C. Majidi, *Advanced Materials Interfaces* **2018-05-01**, *5*, 10 1701596.

[25] E. P. Yalcintas, K. B. Ozutemiz, T. Cetinkaya, L. Dalloro, C. Majidi, O. B. Ozdoganlar, *Advanced Functional Materials* **2019**, *0*, 0 1906551.

[26] E. L. White, J. C. Case, R. K. Kramer, *Sensors and Actuators A: Physical* **2017-01-01**, *253* 188.

[27] K. Kim, J. Choi, Y. Jeong, M. Kim, I. Cho, S. Kim, Y. Oh, I. Park, In *2019 20th International Conference on Solid-State Sensors, Actuators and Microsystems Eurosensors XXXIII (TRANSDUCERS EUROSENSORS XXXIII)*. **2019-06** 2535–2538.

[28] M.-g. Kim, H. Alrowais, O. Brand, *Advanced Electronic Materials* **2018**, *4*, 2 1700434.

[29] S. J. Mazlouman, X. J. Jiang, A. N. Mahanfar, C. Menon, R. G. Vaughan, *IEEE Transactions on Antennas and Propagation* **2011**, *59*, 12 4406, conference Name: IEEE Transactions on Antennas and Propagation.

[30] G. B. Zhang, R. C. Gough, M. R. Moorefield, K. J. Cho, A. T. Ohta, W. A. Shiroma, *IEEE Antennas and Wireless Propagation Letters* **2018**, *17*, 1 50, conference Name: IEEE Antennas and Wireless Propagation Letters.

[31] K. L. Dorsey, In *2019 2nd IEEE International Conference on Soft Robotics (RoboSoft)*. **2019-04** 378–383.

[32] W. Shan, T. Lu, C. Majidi, *Smart Materials and Structures* **2013**, *22*, 8 085005.

[33] W. Shan, S. Diller, A. Tutcuoglu, C. Majidi, *Smart Materials and Structures* **2015**, *24*, 6 065001.

[34] S. H. Jeong, K. Hjort, Z. Wu, *Scientific Reports* **2015-02-12**, *5*, 1 8419, number: 1 Publisher: Nature Publishing Group.

[35] S. Guo, P. Wang, J. Zhang, W. Luan, Z. Xia, L. Cao, Z. He, *Frontiers in Energy* **2019-09-01**, *13*, 3 474.

[36] N. Lazarus, B. Hanrahan, *Advanced Materials Technologies* **2016**, *1*, 8.

[37] R. Guo, L. Sheng, H. Gong, J. Liu, *Science China Technological Sciences* **2018-04-01**, *61*, 4 516.

[38] T. N. Do, H. Phan, T. Nguyen, Y. Visell, *Advanced Functional Materials* **2018**.

[39] M. Naghdi, F. Farzbod, P. M. Goggans, In *ASME 2019 International Mechanical Engineering Congress and Exposition*. American Society of Mechanical Engineers Digital Collection, **2020-01-21** URL `https://asmedigitalcollection.asme.org/IMECE/proceedings/IMECE2019/59476/V010T12A017/1073510`.

[40] S. W. Jin, J. Park, S. Y. Hong, H. Park, Y. R. Jeong, J. Park, S.-S. Lee, J. S. Ha, *Scientific Reports* **2015-07-16**, *5*.

[41] G. M. Whitesides, *Angewandte Chemie International Edition* **2018**, *57*, 16 4258, _eprint: https://onlinelibrary.wiley.com/doi/pdf/10.1002/anie.201800907.

[42] P. Polygerinos, N. Correll, S. A. Morin, B. Mosadegh, C. D. Onal, K. Petersen, M. Cianchetti, M. T. Tolley, R. F. Shepherd, *Advanced Engineering Materials* **2017**, *19*, 12 1700016, _eprint: https://onlinelibrary.wiley.com/doi/pdf/10.1002/adem.201700016.

[43] A. D. Marchese, R. K. Katzschmann, D. Rus, *Soft Robotics* **2015**, *2*, 1 7, publisher: Mary Ann Liebert, Inc., publishers.

[44] H. He, S. Lv, W. Liu, Z. Sun, X. Kang, C. Niu, In *2017 4th International Conference on Electric Power Equipment - Switching Technology (ICEPE-ST)*. **2017** 514–518.

[45] H. O. Michaud, S. P. Lacour, *APL Materials* **2019**, *7*, 3 031504, publisher: American Institute of Physics.

[46] Y.-G. Park, H. S. An, J.-Y. Kim, J.-U. Park, *Science Advances* **2019**, *5*, 6 eaaw2844, publisher: American Association for the Advancement of Science Section: Research Article.

[47] Y.-G. Park, H. Min, H. Kim, A. Zhexembekova, C. Y. Lee, J.-U. Park, *Nano Letters* **2019**, *19*, 8 4866, publisher: American Chemical Society.

[48] J. Black, *IEEE Transactions on Electron Devices* **1969-04**, *16*, 4 338.

[49] J. Black, *Proceedings of the IEEE* **1969-09**, *57*, 9 1587.

[50] D. G. Pierce, P. G. Brusius, *Microelectronics Reliability* **1997-07-01**, *37*, 7 1053.

[51] P. S. Ho, T. Kwok, *Reports on Progress in Physics* **1989-03**, *52*, 3 301.

[52] F. T. von Kleist-Retzow, O. C. Haenssler, S. Fatikow, *Journal of Microelectromechanical Systems* **2019-02**, *28*, 1 88.

[53] J. Je, J. Lee, *Journal of Microelectromechanical Systems* **2014**, *23*, 5 1156, conference Name: Journal of Microelectromechanical Systems.

[54] M. Liu, J. Sun, Q. Chen, *Sensors and Actuators A: Physical* **2009-04-08**, *151*, 1 42.

[55] Ecoflex™ 00-30 product information, URL `https://www.smooth-on.com/products/ecoflex-00-30/`, Library Catalog: www.smooth-on.com.

[56] T. Lu, L. Finkenauer, J. Wissman, C. Majidi, *Advanced Functional Materials* **2014**, *24*, 22 3351.

[57] M. Jason T. Rich, M. J. Gail Neely, M. Randal C. Paniello, M. D. Courtney C. J. Voelker, M. Brian Nussenbaum, M. Eric W. Wang, *Otolaryngology–Head and Neck Surgery* **2010**, *143*, 3 331, pMID: 20723767.

[58] M. Knoblauch, J. M. Hibberd, J. C. Gray, A. J. E. van Bel, *Nature Biotechnology* **1999**, *17*, 9 906, number: 9 Publisher: Nature Publishing Group.

[59] N. Bowden, W. T. S. Huck, K. E. Paul, G. M. Whitesides, *Applied Physics Letters* **1999**, *75*, 17 2557, publisher: American Institute of Physics.

[60] M. A. H. Khondoker, A. Ostashek, D. Sameoto, *Advanced Engineering Materials* **2019**, *21*, 7 1900060, _eprint: https://onlinelibrary.wiley.com/doi/pdf/10.1002/adem.201900060.

[61] W. Robertson, B. Cazzolato, A. Zander, *IEEE Transactions on Magnetics* **2012-09**, *48*, 9 2479, conference Name: IEEE Transactions on Magnetics.

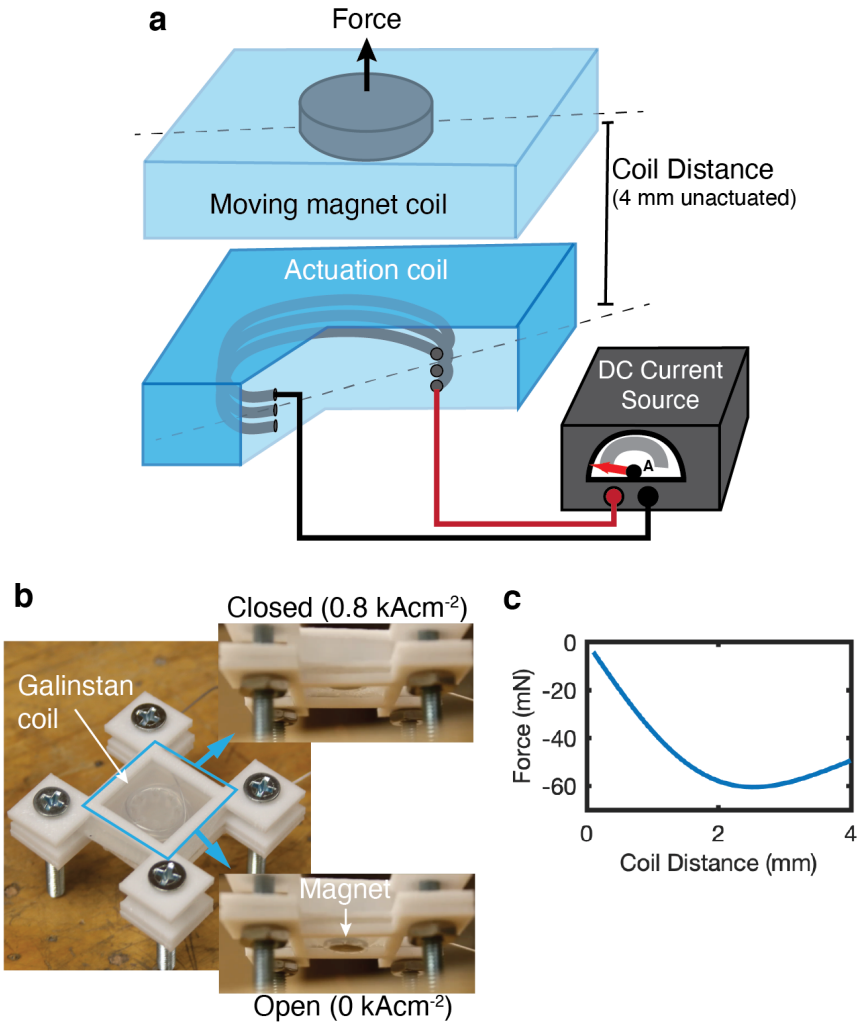

Figure 1: Diagram and operation of the stretchable electromagnet (a) The operating mechanism and coil distance, which is defined from the vertical center line of the magnet to the vertical center line of the coil. The unactuated center-to-center distance is 4 mm. (b) A soft electromagnetic valve with Galinstan coil and permanent magnet. The inset figures show the valve motion with current off (open) and current on (closed). (c) Modeled force on the magnet as a function of center-to-center coil distance for a DC current density of 0.8 $kAcm^{-2}$.

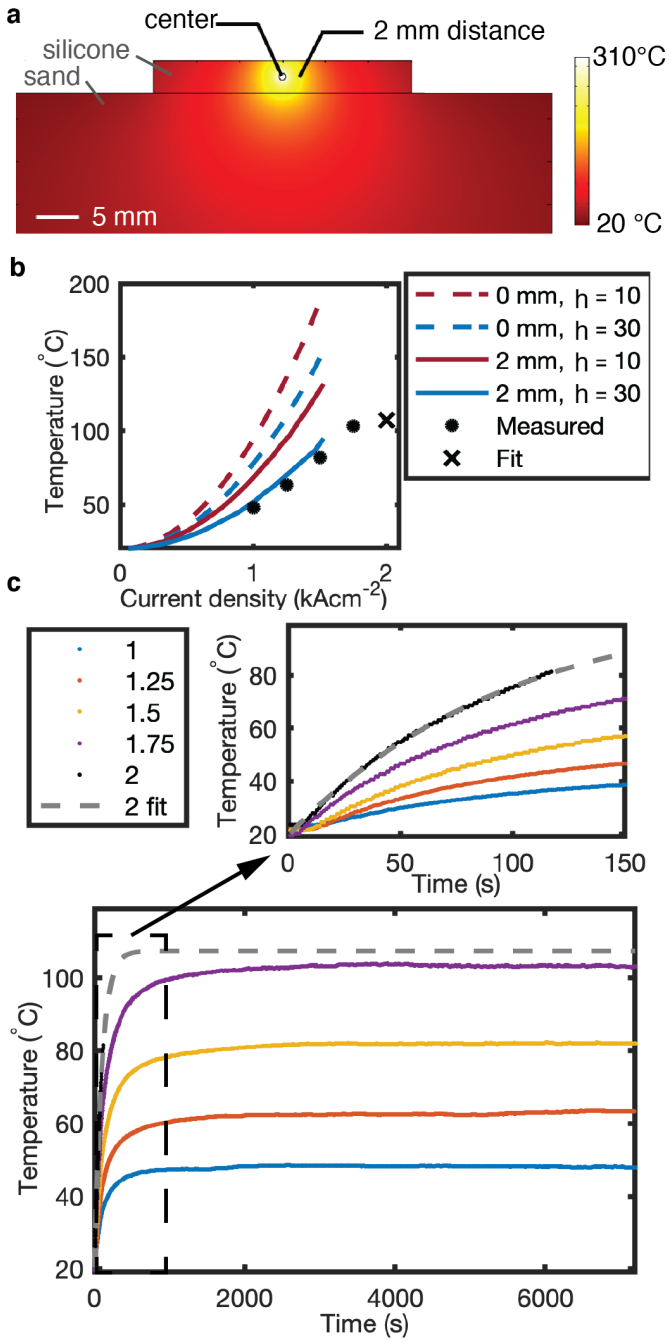

Figure 2: Temperature simulations and measurements of the Galinstan samples. (a) The modeled temperature profile for a liquid metal wire with a current density of 2 kAcm^{-2}. The 310 °C temperature near the center of the wire at this current density suggests limiting current density below 1.5 kAcm^{-2} to prevent silicone decomposition. (b) The relationship between measured, fit, and modeled steady-state temperature and current density. (c) The measured temperature after current step for each current density. An exponential fit is plot for $J = 2$ kAcm^{-2} as every sample failed before reaching its steady-state temperature.

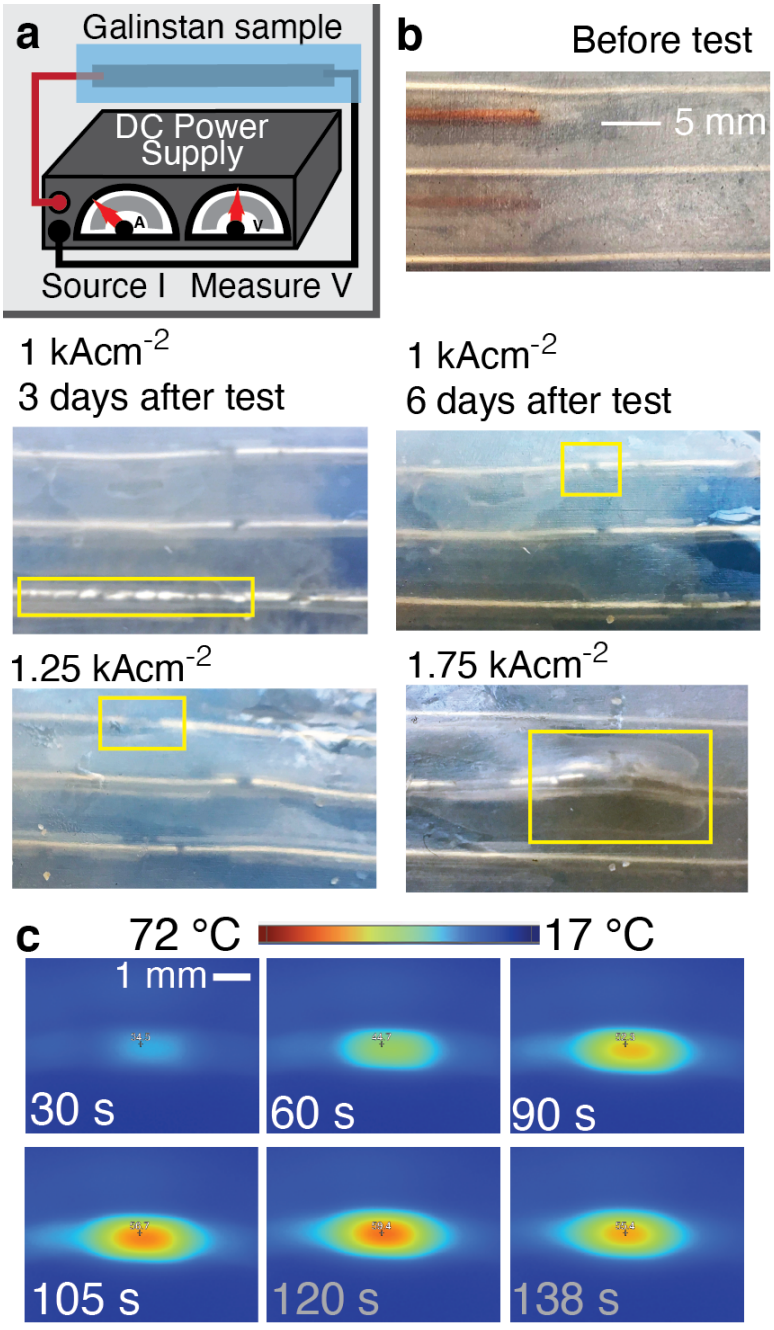

Figure 3: Testing and imaging open circuit failures in Galinstan wires. (a) The test procedure for measuring MTTF, where constant current is sourced from a DC power supply and the voltage across the Galinstan wire is recorded. (b) Photographs of the wires before and after testing. A pre-test sample with embedded thermocouples (top right). Representative post-test voids are highlighted with yellow boxes. The 1 kAcm^{-2} samples show voids three days after test conclusion (middle left), but these voids have largely disappeared six days after test conclusion (middle right). All three wires in a 1.25 kAcm^{-2} sample shown visible breaks in the Galinstan ranging from 1-2 mm width. The middle wire in the 1.75 kAcm^{-2} sample has buckled out of plane and has an approximately 4 mm gap to the left of the buckle (bottom right). (c) A series of infrared thermographs along the wire's length during a 2 kAcm^{-2} test, until failure at t= 108 s.

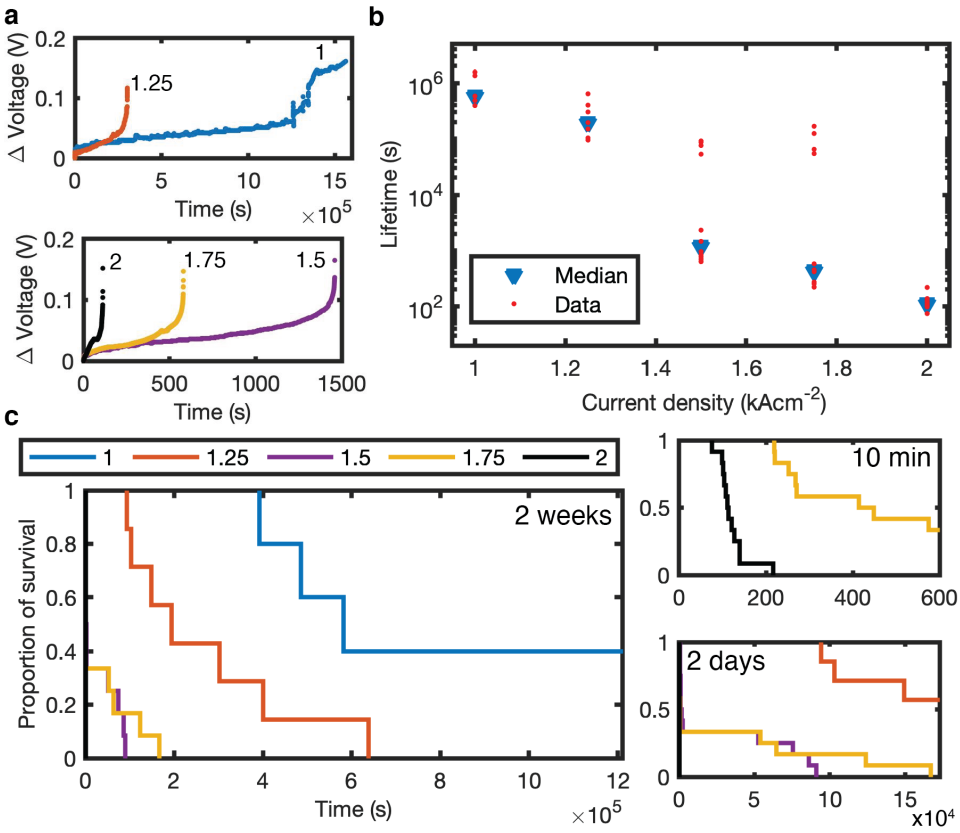

Figure 4: Sample behavior over time and with applied current. (a) Voltage change after current application for a representative sample at each current density. (b) Sample lifetime and median lifetime at each current density. (c) Kaplan-Meier curves showing the proportion of survived devices over two weeks. Inset: Kaplan-Meier curves over 10 minutes and 2 days.

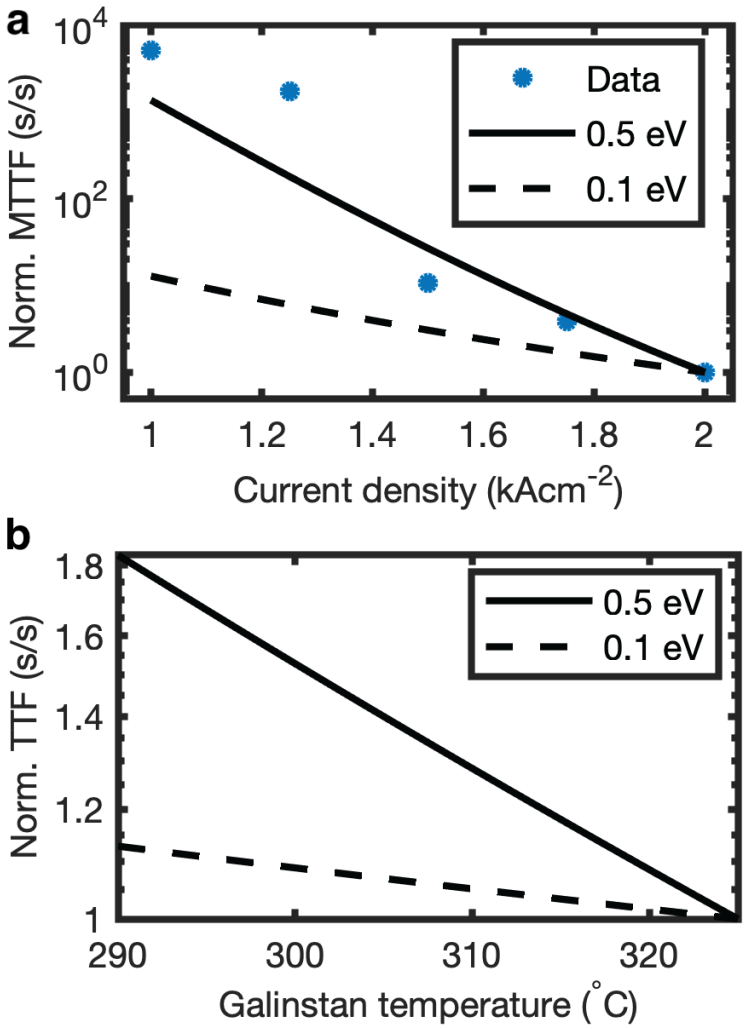

Figure 5: Normalized MTTF due to electromigration for two activation energies (a) MTTF with current density. Each curve represents one value of E_a, with the largest $E_a = 0.5$ eV serving as the values fit to small-crystalline Al [48]. The temperature used in the electromigration model is extracted from the finite element analysis simulation at the center of the wire. (b) Normalized MTTF with Galinstan temperature with current density of 2 kAcm^{-2}. Decreasing sample temperature resulted in a much larger MTTF increase than this model predicts.

Table of Contents

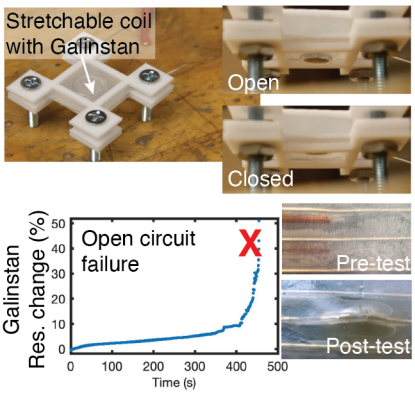

Stable conductors, such as liquid metal filled silicone, must withstand high current densities to meet new applications in electromagnetic actuation, heating, and power transfer. Liquid metal wire lifetime at current densities on the order of 1 kAcm^{-2} are investigated along with the effects of current pulsing and cooling. Liquid metal wire lifetime is current- and temperature-dependent, with lifetime ranging from a median of 112 s to 100 h form current densities of 1-2 kAcm^{-2}. Open circuit failures are visible in the wires after applying current.